ARMY RESEARCH LABORATORY

Experiments in Cold Atom Optics at ARL I: Introduction to Atom Chip Set-up

by Jason Alexander, Christopher Rowlett, Violeta Prieto, William Golding, and Patricia Lee

ARL-TR-5787 **September 2011**

NOTICES

Disclaimers

The findings in this report are not to be construed as an official Department of the Army position unless so designated by other authorized documents.

Citation of manufacturer's or trade names does not constitute an official endorsement or approval of the use thereof.

Destroy this report when it is no longer needed. Do not return it to the originator.

Army Research Laboratory
Adelphi, MD 20783-1197

ARL-TR-5787 **September 2011**

Experiments in Cold Atom Optics at ARL I: Introduction to Atom Chip Set-up

Jason Alexander, Christopher Rowlett, Violeta Prieto, William Golding, and Patricia Lee
Sensors and Electron Devices Directorate, ARL

REPORT DOCUMENTATION PAGE	Form Approved OMB No. 0704-0188

1. REPORT DATE *(DD-MM-YYYY)*	2. REPORT TYPE	3. DATES COVERED (From - To)
September 2011		

4. TITLE AND SUBTITLE	5a. CONTRACT NUMBER
Experiments in Cold Atom Optics at ARL I: Introduction to Atom Chip Set-up	5b. GRANT NUMBER
	5c. PROGRAM ELEMENT NUMBER

6. AUTHOR(S)	5d. PROJECT NUMBER
Jason Alexander, Violeta Prieto, Christopher Rowlett, William Golding, and Patricia Lee	5e. TASK NUMBER
	5f. WORK UNIT NUMBER

7. PERFORMING ORGANIZATION NAME(S) AND ADDRESS(ES)	8. PERFORMING ORGANIZATION REPORT NUMBER
U.S. Army Research Laboratory ATTN: RDRL-SEE-O 2800 Powder Mill Road Adelphi MD 20783-1197	ARL-TR-5787

9. SPONSORING/MONITORING AGENCY NAME(S) AND ADDRESS(ES)	10. SPONSOR/MONITOR'S ACRONYM(S)
	11. SPONSOR/MONITOR'S REPORT NUMBER(S)

12. DISTRIBUTION/AVAILABILITY STATEMENT

Approved for public release; distribution unlimited.

13. SUPPLEMENTARY NOTES

14. ABSTRACT

Gyroscopes based on ultracold atom interferometry have the potential to exhibit an intrinsic sensitivity larger by a factor of 4 x 1010 than for light-based interferometers. One of the major technical challenges for the advancement of atom optics and development of practical guided matter wave interferometers is the realization of coherent beam splitters. The overall focus of our research program is to develop a physical understanding of the conditions needed for coherent beam splitting and transport and use this knowledge to implement atom chip based interferometers using clouds of ultracold atoms. In this report we describe our experimental apparatus in detail and discuss the current progress towards interferometric measurements with clouds of ultracold atoms in a chip-based magnetic waveguide.

15. SUBJECT TERMS

Atom chip, atomic waveguides

16. SECURITY CLASSIFICATION OF:			17. LIMITATION OF ABSTRACT	18. NUMBER OF PAGES	19a. NAME OF RESPONSIBLE PERSON
a. REPORT	b. ABSTRACT	c. THIS PAGE			Jason Alexander
UNCLASSIFIED	UNCLASSIFIED	UNCLASSIFIED	UU	28	19b. TELEPHONE NUMBER (*Include area code*) (301) 394-1919

Contents

List of Figures

INTENTIONALLY LEFT BLANK.

1. Introduction

The temperature of a normal atomic gas is proportional to the mean-squared atomic velocity. In his Ph.D. dissertation work, Louis deBroglie proposed that atoms and molecules, just like light, have associated wave properties that are purely quantum mechanical in nature (*1*). The fundamental quantity that describes the wave nature of matter is the particle's deBroglie wavelength which depends on its mass and velocity. Albert Einstein, building on the work of S. N. Bose, predicted in 1924 that when atoms are slow enough and close enough together that the mean distance between atoms in longer than an individual atom's deBroglie wavelength, a new state of matter is created, now called a Bose-Einstein condensate (BEC). In 1995, the first Bose-Einstein condensate was finally realized experimentally in a dilute vapor of alkali atoms (*2*) by combining the techniques of laser cooling and trapping (*3*) and radio frequency evaporation (*4*). In a Bose-Einstein condensate, all of the atoms in the condensate occupy a single quantum state such that the macroscopic motion of each atom in the condensate is described by the same quantum mechanical wave-function. In an atom interferometer employing Bose condensed atoms, the spatially separated clouds of condensate atoms are confined and guided by magnetic, electric, or optical fields and propagate in different directions in the interferometer. While separated, the atom clouds will obtain different quantum phases and, upon recombination, will produce an interference pattern. This interference pattern can provide information about the external conditions influencing each atom wave-packet in the interferometer, such as rotation, linear acceleration, electric, and magnetic fields.

Recent interferometer experiments with thermal atoms falling freely under the influence of gravity obtained sensitivities on par with current state-of-the-art gyroscopes (*5*). However, a guided wave interferometer using BECs could be able to increase the sensitivity of inertial sensors ten orders of magnitude beyond these experiments. Moreover, such an interferometer can be scaled down both in size and power requirements to allow a practical, portable sensor based on this physical phenomenon.

Rotation sensing requires that two halves of the initial wave packet propagate around a path that encloses an area. If the interferometer is rotating, then the Sagnac effect produces opposite phase shifts in the two wave packets, where the phase shifts are proportional to both the rotation rate and the area enclosed by the paths traversed by the wave packets. Measurements of the phase difference between the two wave packets can then be used to determine the rotation rate. It has been shown that guided atoms can circulate around a closed path with an effective area as large as 4400 mm^2 (*6*). However, in that experiment the atom sample could not easily be split into two counter-propagating wave packets and therefore, the phase difference (rotation rate) could not be determined. Thus, one of the major technical challenges for the advancement of atom optics and development of practical guided matter wave interferometers is the realization of

coherent beam splitters. The latest technological innovation in atom optics has been the development of so-called atom chips (*7*). Figure 1 shows the chip currently used in our experimental system (*8*). Atom chips consist of micro-fabricated wire structures on the chip surface that are used to generate magnetic guiding and trapping potentials. These potentials confine ultra-cold atoms near the surface of the chip for coherent manipulation by external bias and/or laser fields. Because of the small size, magnetic field gradients that typically require ~10 A in a free space atom guide or trap can be accomplished on the chip with ~10mA. In addition to magnetic trapping potentials, lasers and other electro-optical elements can be integrated on an atom chip, allowing the development of compact, portable devices.

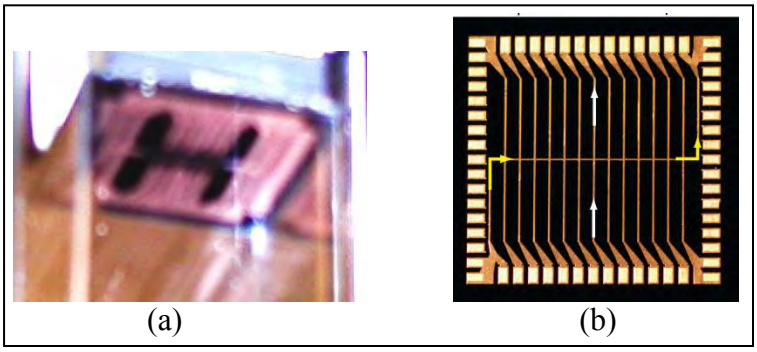

Figure 1. Current atom chip used in our system. (a) Chip mounted on ultra-high vacuum cell, viewed from below (b) Enlarged image of atom chip detailing micro-fabricated wire structures on the chip surface that are used to generate magnetic guiding and trapping potentials (*8*).

To date, the successful use of atom chip based interferometers as inertial sensors has been hindered by the ability to split the atom beam into coherent parts and have an effective means of reading out the phase information. The overall focus of our research program is to overcome these technical challenges and implement atom chip interferometers using clouds of BEC atoms. In this report we describe our experimental apparatus in detail and discuss the current progress towards interferometric measurements with clouds of ultra-cold atoms on a chip.

2. Laser Cooling and Trapping

Fundamental to the successful implementation of atom interferometry is the ability to cool atoms to within a billionth of a degree above absolute zero. Figure 2 shows the relevant temperature scale involved. Cooling atoms to this low temperature requires a combination of techniques. Excellent descriptions of the physics of laser cooling and trapping as well as Bose-Einstein condensation may be found in (*3*), therefore, here we will only briefly review the physics of laser cooling and trapping that lead to the production of the macroscopic atom trap which is used to

load the chip trap. The process of evaporative cooling and some properties of the Bose-Einstein condensate relevant to interferometry in the chip wave-guide will be discussed in section 3.4.

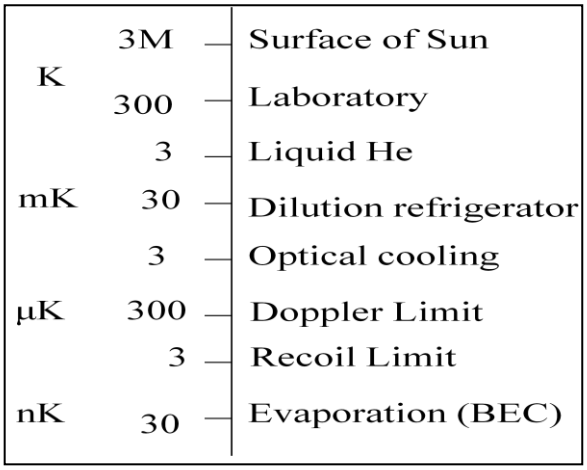

Figure 2. Relevant temperature scales for cooling and trapping atoms.

2.1 Doppler Cooling

In 1975 it was suggested that atoms in a low-density vapor could be slowed via radiation pressure, and thus provide the ability to manipulate the external degrees of freedom of an individual atom (*9*). The mechanism proposed in that work is Doppler cooling. Atoms traveling in a laser field detuned to the red of an atomic resonance transition will preferentially absorb photons opposing their motion. These photons are tuned into resonance by the Doppler shift. After an atom absorbs a photon, it will re-emit the photon via either stimulated or spontaneous emission. Stimulated emission is an elastic process and leaves the laser-atom system unchanged. The direction of a spontaneously emitted photon, however, is random and spatially symmetric. Therefore, a net force occurs after many absorption and emission cycles. The net force on an atom in a laser field that is detuned by Δ_o from an atomic transition is given by,

$$F = \frac{\Gamma \hbar k}{2} \frac{2\Omega^2}{2\Omega^2 + 4\Delta^2 + 1} \tag{1}$$

where ħk is the momentum of the atom, $\Omega = I/I_{sat}$, I is the laser intensity, I_{sat}, is the saturation intensity of the atomic transition, $\Delta = \Delta_o - \vec{k} \cdot \vec{v}$ is the net detuning of the laser including the Doppler shift, and $\vec{v}$ is the velocity of the atom. From this we see that atoms, that have velocity components opposing the wave vector of the laser beam, see resonant light as the detuning is shifted into resonance by the Doppler shift. These atoms will experience a greater force than those moving away from the laser. The lower limit, T_D, on the temperature that can be reached via Doppler cooling is determined by the energy uncertainty in the excited state, $\hbar\Gamma$, and is given by

$$T_D = \frac{\hbar \Gamma}{2K_B} \tag{2}$$

where Γ is the natural linewidth of the atomic transition and K_B is the Boltzmann constant. For Doppler cooling using the $5s_{1/2} \rightarrow 5p_{3/2}D_2$ line in ^{87}Rb, which has a natural linewidth of ~6 MHz, the Doppler limit is T_D=144μK. Sub-Doppler cooling techniques allow one to cool atoms below the Doppler limit described above. These techniques include adiabatic cooling, Raman cooling, velocity selective coherent population trapping (VSCPT) and polarization gradient cooling (*3*). These cooling mechanisms reach temperatures near the recoil limit,

$$T_R = \frac{(\hbar k)^2}{K_B m}, \tag{3}$$

where k is the photon wavevector and m is the atomic mass. T_R is the temperature associated with the velocity given to an atom due to the recoil of a single spontaneous emission. For ^{87}Rb T_R~0.4 μK.

2.2 Magneto-optical Trap

The most common type of optical trap is the magneto-optical trap (MOT). A MOT is a configuration of three pairs of counter-propagating laser beams with orthogonal circular polarizations. Initially Doppler cooling slows atoms in all spatial dimensions. Once the atoms are slowed sufficiently, sub-Doppler mechanisms, such as polarization gradient cooling, take over. This configuration is known as the optical molasses. These atoms have been slowed (cooled) significantly, but are not yet trapped. In order to trap the atoms an inhomogeneous magnetic field is applied via a pair of coils in an anti-Helmholtz configuration. Atoms that drift away from the magnetic minimum are shifted into resonance with a laser beam that is anti-parallel to the atomic motion via the Zeeman effect. Therefore, the gradient of the applied magnetic field provides a spatial dependence to the optical force. The MOT has a very large velocity capture range, and can produce densities of 10^8–10^{11} cm^{-3} at temperatures near 1 mK.

3. Experimental Set-Up

Figure 3 shows an overview of the experimental steps required to produce a Bose-Einstein condensate on the atom chip in our current system. In the following sections, we will describe the details of the experimental set-up and process involved in loading the atom chip trap. In section 3.1, we will discuss stabilization of the frequency of the various lasers required for the experiment. In section 3.2 we will describe the 2-D and 3-D MOT arrangement specific to our system. Section 3.3 will describe the external Z-wire trap which allows the transfer of atoms from the 3D-MOT to the atom chip trap. Section 3.4 will cover the chip dimple trap, evaporative cooling in the chip dimple trap, and interferometry in the chip waveguide.

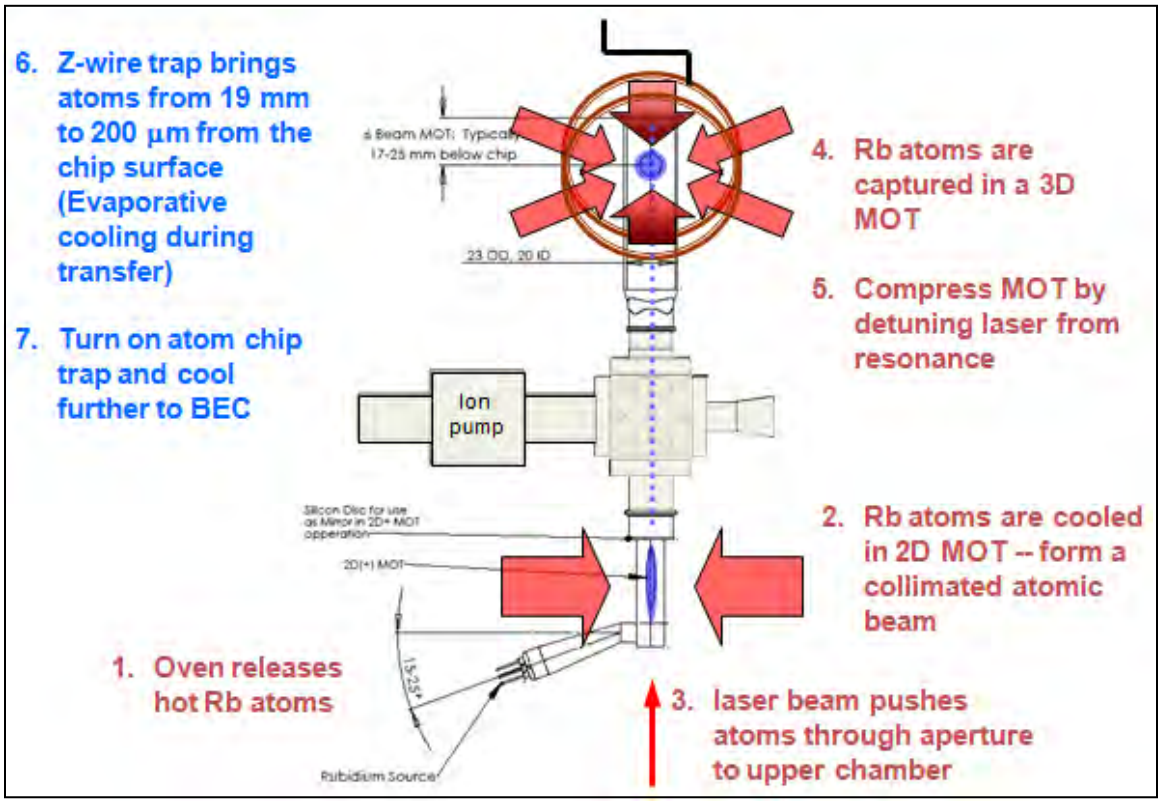

Figure 3. Overview of steps required to produce BEC on a chip in current system.

3.1 Laser Frequency Stabilization

The experiment requires three different wavelengths of laser light: two to make the magneto-optical trap and one to image the condensate. For the MOT's trapping beams we use a commercial external cavity diode laser (Toptica DL Pro), which is amplified by a single pass through a tapered amplifier (Toptica BoosTA), in a master-oscillator power amplifier (MOPA) configuration. The hyperfine repump beam is supplied by a separate MOPA arrangement (Sacher). These lasers must be frequency stabilized to <6 MHz in order to have a stable MOT from which to load the chip trap. To do this we lock both the cooling laser and the repump laser to a reference "master" laser which is locked to atomic transitions in ^{87}Rb via saturated absorption spectroscopy. The basic idea is to produce sub-Doppler spectral lines which can be used as feedback to stabilize the laser. To determine laser frequency, the saturated absorption lock exploits the strong frequency dependence of atomic absorption. As laser frequency is swept through the atomic resonance, the absorption grows rapidly (and conversely, transmission through the vapor cell falls) in a Gaussian-shaped profile with the peak of the Gaussian at the resonance frequency. If the atoms were stationary along the beam path, the absorption profile would be a narrow Lorentzian function on the resonance. However, the motion of the atoms is in fact random, with velocity components along the path of the laser beam. Due to the Doppler effect, the frequency of the light is shifted as $\omega_- = \omega_0 - kv$ for atoms moving parallel to the beam, and $\omega_+ = \omega_0 + kv$ for atoms moving antiparallel to the beam. While a Doppler broadened

profile is typically hundreds of MHz wide, we would like to stabilize our laser frequency to within a few MHz. This can be accomplished by exploiting the phenomenon of saturation. The rate at which an atom scatters photons is

$$R_s = \frac{\Gamma}{2}\left(\frac{I/I_{sat}}{1+\frac{I}{I_{sat}}+4\frac{\Delta^2}{\Gamma^2}}\right) \tag{4}$$

where I is the total incident radiation intensity, Δ is the detuning of the laser light from resonance, Γ is the natural linewidth, and I_{sat} is the saturation intensity. As the laser detuning is decreased, the Δ term approaches zero. As laser intensity is increased, the scattering rate R_s approaches a maximum of $\Gamma/2$. The optical layout for saturated absorption spectroscopy is shown in figure 4. Two weak probe beams travel through a vapor cell. A counter-propagating pump beam, which is at approximately saturation intensity, crosses one of the probe beams as it passes through the vapor cell. As laser frequency is swept through an atomic resonance, each probe beam exhibits a Doppler-broadened absorption profile. The counter-propagating pump beam will also exhibit a Doppler profile, however, atoms moving parallel to the pump beam are moving antiparallel to the probe beams. Therefore, the pump and probes do not interact with the same population of atoms at the same time. The exception is the group of atoms with zero velocity along the beam path.

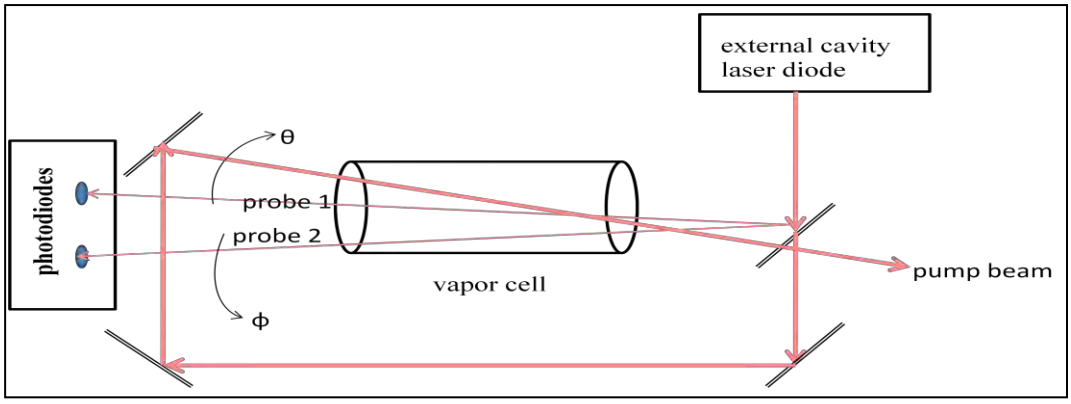

Figure 4. Laser beam path in saturated absorption spectroscopy. The input beam is sent to a wedge, which reflects two weak beams with an angle φ between them, and transmits a stronger beam. The weak probe beams pass directly through the vapor cell, to the photodiodes. The strong pump beam is carried around the cell, and enters from the opposite side so that it opposes the probe beams. The pump crosses only one of the probes while traversing the vapor cell. The saturated absorption signal is optimized when the angle θ between pump and probe is minimized.

These atoms will interact simultaneously with pump and probe beams. The pump beam is intense enough to saturate the atoms, so that they will absorb very little light from the weaker probe beam. The sudden drop in absorption results in a sharp, Doppler-free feature at the resonant frequency, as shown in figure 5 for an ideal two-level system. This peak sits on top of the Doppler profile, but by subtracting this signal from the other probe beam, we can isolate the Doppler-free feature, and produce the saturated absorption signal.

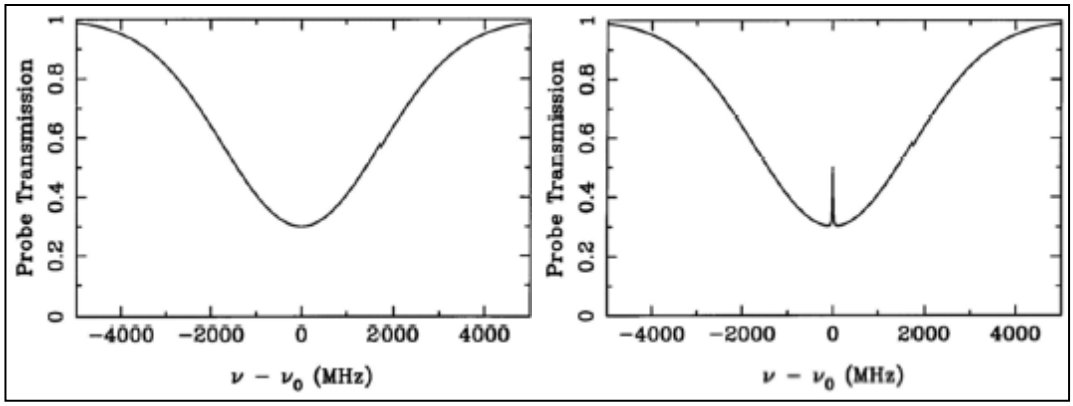

Figure 5. Example of saturated absorption in a two-level system. Each graph is the absorption profile of a probe beam. The first probe does not cross the pump beam, so it exhibits a normal Doppler-broadened profile. The second probe crosses the pump while traveling through the vapor cell, resulting in a sharp increase in probe transmission at the atomic resonance. By subtracting one signal from the other, we isolate the Doppler-free feature and create a saturated absorption trace (*10*).

In a multi-level atom, the ground state and excited state may have hyperfine levels that are very closely spaced. In a multi-level atom, the saturated absorption spectrum is more complicated. For example, take the absorption spectrum of an atom such as rubidium, with one ground state and two closely spaced excited states, as shown in figure 6. The first feature occurs at ν_1, the frequency of the transition between the ground state and the first excited state. The third feature occurs at ν_2, the frequency of the transition between the ground state and the second excited state. The middle feature occurs at $(\nu_1 + \nu_2)/2$, and is called a "cross-over resonance". This peak arises because there is a group of atoms with velocity such that the Doppler shift brings the pump into resonance with one transition and the probe into resonance with the other. These atoms can interact with either beam, so that the observed feature is at the average of the two frequencies.

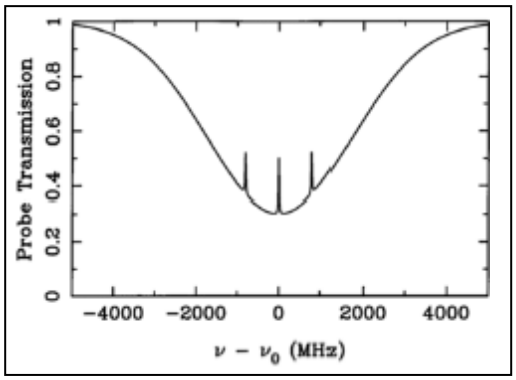

Figure 6. Example of saturated absorption in a multi-level system. The first feature occurs at ν_1, the frequency of the transition between the ground state and the first excited state. The third features occur at ν_2, the frequency of the second excited state. The middle feature occurs at $(\nu_1 + \nu_2)/2$, the average of the frequencies of the two excited states, because atoms in the proper velocity group find the pump beam Doppler-shifted to one transition and the probe beam Doppler-shifted to the other (*10*)

We lock each laser to the peak atomic transition. Unfortunately, a servo can only lock to a region where there is a slope of the line to use as feedback. The standard solution to this problem is to generate a derivative of the saturated absorption signal. We modulate the frequency of the laser by modulating the electrical current driving the laser. The modulation rate is 90 kHz, which is slow enough for the laser to respond, but fast enough to be above the band width of the servo. The signal from the saturated absorption spectrometer is sent to a lock-in amplifier which gives the derivative of the original transition lines. The derivative changes sign at the absorption peak, and thus when compared to a zero-volt reference, is a convenient error signal for a servo. An energy level diagram for the ^{87}Rb D_2 line is shown in figure 7. We lock our master laser (New Focus Vortex) at the cross-over between the |F=2, F'=2> and the |F=2, F'=3> transition, which is 133.5 MHz to the red of the |F=2, F'=3> cooling transition at 780.2460 nm. This master laser is used as a reference oscillator for locking both the repump and cooling lasers.

The servo signal for the cooling and repump laser locks are generated via optical heterodyne. In this technique, light from the master laser and from the cooling or repump laser are combined on a photodiode. The resulting rf beat-note signal from the interference of the two optical signals is then converted to a proportional voltage via homodyne and used as the feedback signal for the lock servo. The cooling laser is initially locked to the F=2, F'=3 transition at 780.460 nm, while the repump laser is locked near the F=1, F'=1 transition at 780.233 nm.

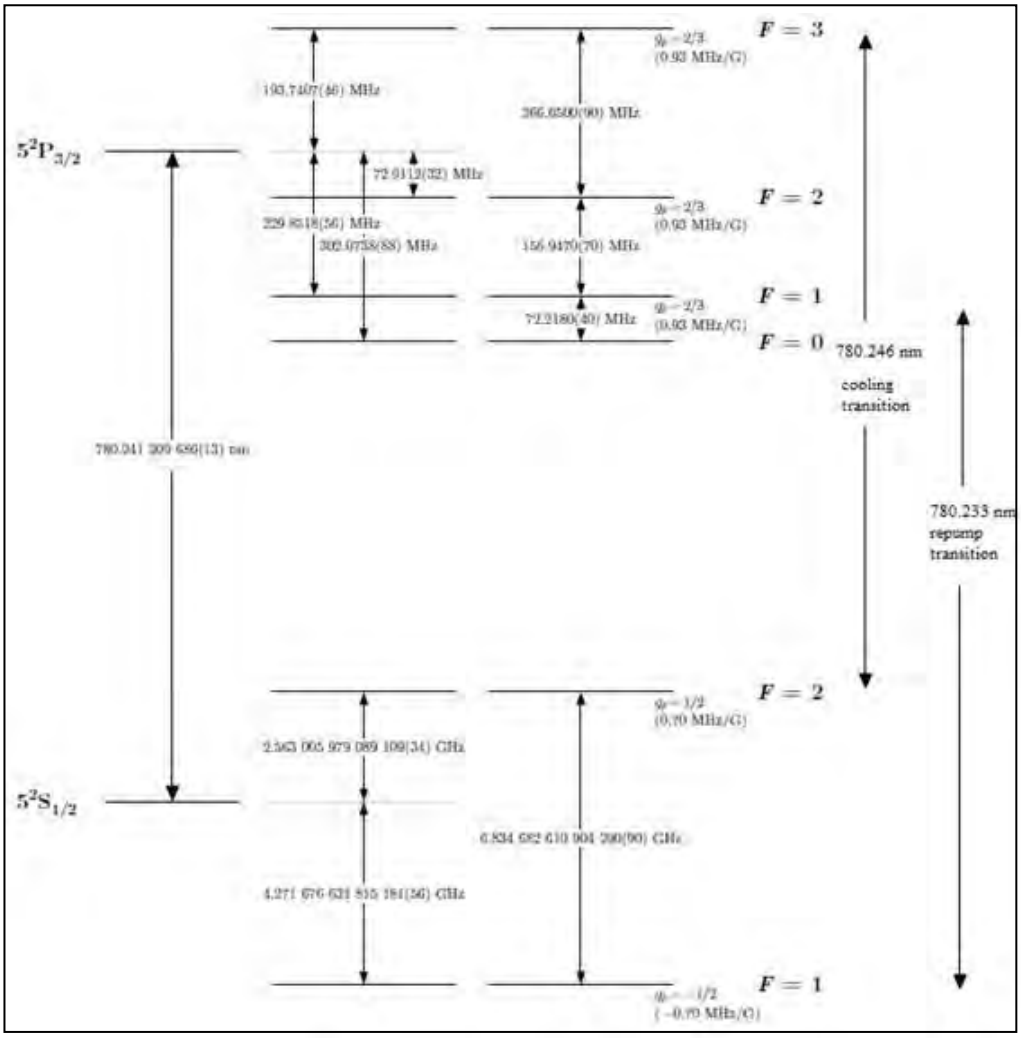

Figure 7. ^{87}Rb D_2 hyperfine structure. Adapted from (*10*)

3.2 2-D and 3-D MOT

The vacuum cell is a two-chamber quartz design produced by Cold Quanta, Inc. (*8*) This system was chosen over the initial in-house design and construction in order to focus on understanding the physics and technical requirements of interferometry on the atom chip, with the creation of both new packages and new atom chips left as a future goal of the group. The upper region, where experiments take place, labeled 3D MOT in figure 8, and the lower 2-D MOT region are separated by a silicon disk with a 750 μm hole which creates differential pumping between the two regions. As a result, ultra-high vacuum conditions are maintained in the 3-D MOT region. Also shown in figure 8 are the associated optics for the 2-D and 3-D MOT and the atom chip, which will be discussed in detail below.

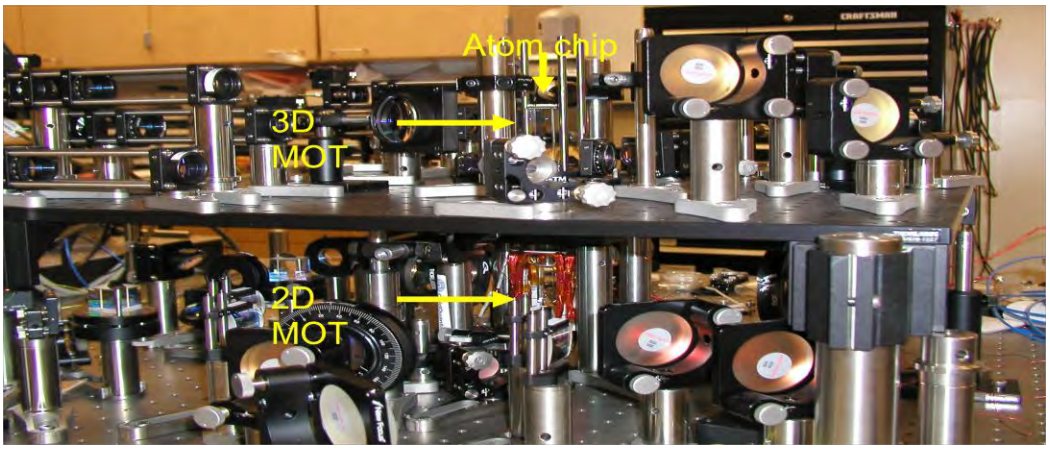

Figure 8. Two-chamber cell used in our system and associated optics. In this image the 3-D MOT coils have been removed for a clearer view of the upper cell.

An expanded view of the 2-D MOT region is shown in figure 9. This lower rectangular cell is 25 mm by 10 mm. Rubidium atoms are introduced into the system via a non-evaporable getter source which creates a Rb pressure between 10^{-8} and 10^{-7} Torr. A pair of cylindrically focused, circularly polarized, and retro-reflected beams with approximately 50 mW of cooling power and 10 mW of repump power are combined with the quadrupole field created by four rectangular magnetic coils of dimension 34.9 mm x 25.4 mm x 6.3 mm and 80 turns of 23 AWG wire which carry approximately 1A of current to produced a 2-D magneto-optical trap. The atoms are unconfined in the vertical direction, and cold Rb atoms are pushed upward through the hole in the silicon disc by an additional laser beam. Reflection of this laser beam off the silicon disc around the hole provides further cooling in the lower chamber, forming a 2D+ MOT (*12*).

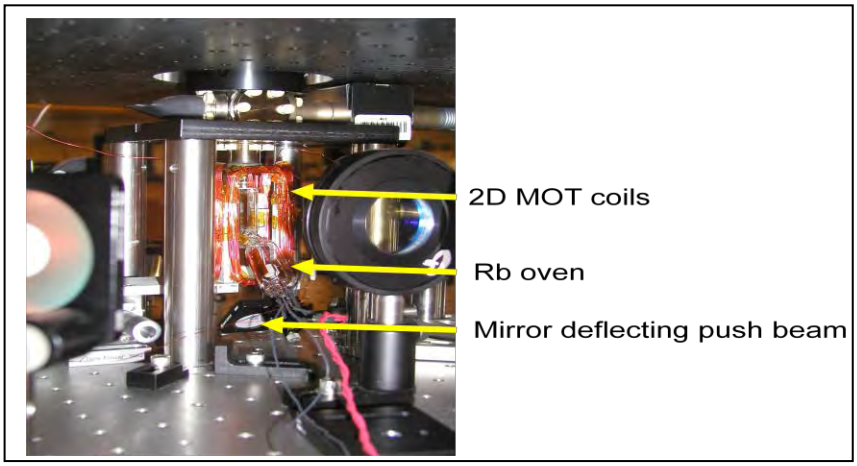

Figure 9. Expanded view of the 2-D+ MOT region. A non-evaporable getter source creates Rb pressure between 10^{-8} and 10^{-7} Torr. Four Cylindrically focused laser beams and four rectangular magnet coils carry ~1 A of current to produce the 2-D MOT. A fifth beam, the push beam, is steered vertically to push atoms into the upper chamber and provide additional cooling.

An overall picture of the 3-D MOT region and associated optics is shown in figure 10 (a). This upper rectangular cell is 70 mm by 22 mm. The 3-D MOT is created by the overlap of a magnetic field gradient and laser beams. Laser light from the repump laser and the cooling laser are combined in a 2x6 fiber splitter and sent to the 3-D MOT region. These fibers are connected to six launchers/beam expanders consisting of an f=6.45 mm asphere, an f=175 mm plano-convex lens, and a λ/2 wave-plate, constructed using Thorlabs' cage mount system which deliver linearly polarized beams with a $1/e^2$ diameter ~18 mm to the 3-D MOT region. Two pairs of beams are steered at a relative angle 2θ=30°, dashed lines in figure 10 (b), and a pair of horizontal beams, into and out of page in figure 10 (b), are overlapped approximately 19 mm from the surface of the atom chip in the center of the upper cell. The beams are circularly polarized with a λ/4 wave-plate just before entering the cell such that anti-parallel beams have opposite polarization. The magnetic field required is generated by coils of dimension 63.5 mm x 38.1 mm x 12.7 mm and 225 turns of 23 AWG wire in an anti-Helmholtz configuration. The current is adjusted in these coils until the overlap between the laser beams and the magnetic field minimum is optimized based on the number and temperature of atoms in the 3-D MOT.

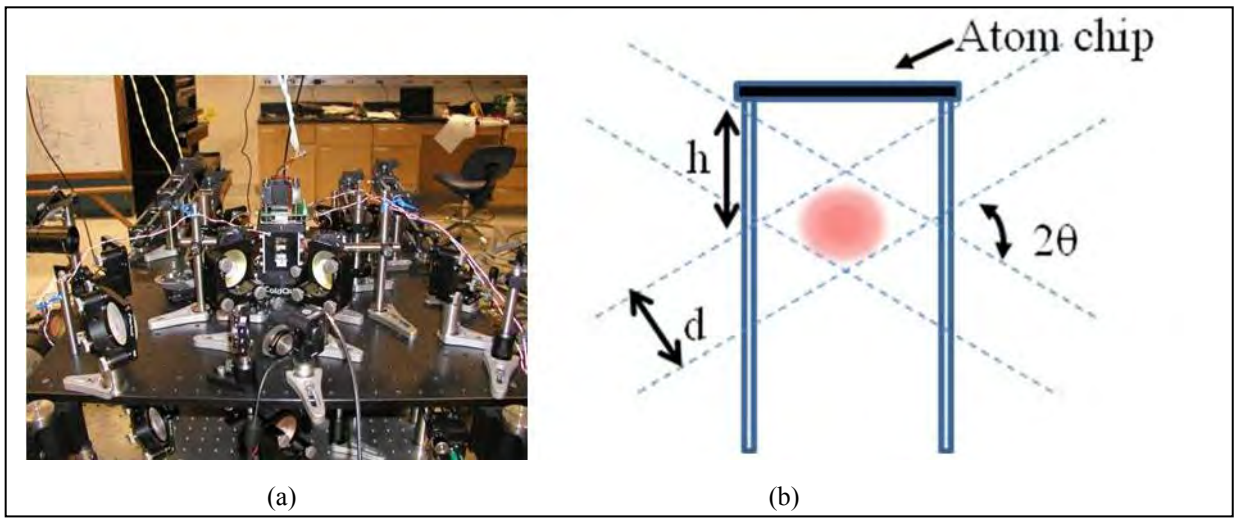

Figure 10. (a) 3-D MOT region and associated optics. A pair of coils in an anti-Helmholtz configuration generate the quadrapole trapping fields. While two pairs of coils in Helmhotz configuration provide bias fields. (b) Two pairs of angled (2θ~30°) beams (dashed lines) of $1/e^2$ diameter d~18 mm and one pair of horizontal beams (into and out of the page) provide the optical cooling for creation of the 3-D MOT a distance h~19 mm from the surface of the atom chip.

Figure 11 shows a typical fluorescence image of the 3-D MOT. Here the entire cell is shown to give a sense of scale for the MOT. From the total pixel intensity and calibrating this with a laser beam of known power incident on the camera, we can obtain the number of atoms in the 3-D MOT via the expression

$$N_{atoms}^{fluorescence} = \frac{4\pi P_{ccd}}{\Omega_s R_s E_{photon}} \quad (5)$$

where E_{photon} is the photon energy, Ω_s is the solid angle for detection, P_{ccd} is the total power collected by the ccd taking into account the quantum efficiency of the camera at 780 nm, and R_s is the photon scattering rate given by equation 4.

Figure 11. Typical fluorescence image of the 3-D MOT. The cloud in this image contains ~$2x10^8$ atoms at a temperature ~300μK.

The temperature of the cloud can be determined by time-of-flight imaging. This is done by turning off the 3-D MOT fields and light and letting the atom cloud undergo a free expansion. Since the density of atoms in a thermal cloud follows a Gaussian distribution, we can perform a Gaussian fit of the cloud image to determine the mean radius of the cloud, *r*. The Gaussian width *w* is related to the mean radius of the cloud by $w^2 = 2\langle r^2 \rangle$. We can take the *w's* from a series of images for different expansion times and fit to the function $w^2 = \alpha + \xi t^2$ and determine the mean square velocity $\xi = 2\langle v^2 \rangle$. The temperature is then related to the mean square velocity through conservation of energy as,

$$T = \frac{m\xi}{2K_B} \tag{6}$$

where m is the mass of a ^{87}Rb atom and K_B is the Boltzmann constant. This technique is an example of time-of-flight (TOF) imaging and is used extensively in cold atom experiments.

3.3 External Z-wire Trap

Due to the finite range of the atom chip trapping potential loading atoms directly from the 3-D MOT into the atom chip trap ~19 mm away is not possible. In order to accomplish loading of the chip trap we use a macroscopic magnetic trap created by a larger external Z-wire and bias fields. Figure 12 (a) shows the top of this external z-wire and its mount, while figure 12 (b) is a close up view of the portion of the wire that faces the top of the atom chip. Also shown is the 13.5 mm diameter wire loop that is used for RF forced evaporation as discussed in section 3.4 below. The external Z-wire consists of 36 turns of 22 AWG wire and the distance between the "legs" of the Z is ~28 mm. In addition two 0.55 mm x 0.2 mm "compression" wires are placed ~.5 mm from the legs of the Z to aide in the transfer of atoms from the external Z-wire trap to the

chip trap discussed in section 3.4 below. Also shown in figure 12 is a finite element model of the magnetic field generated along the center of the upper cell (c) just after transfer from CMOT and (d) just before transfer to atom chip trap.

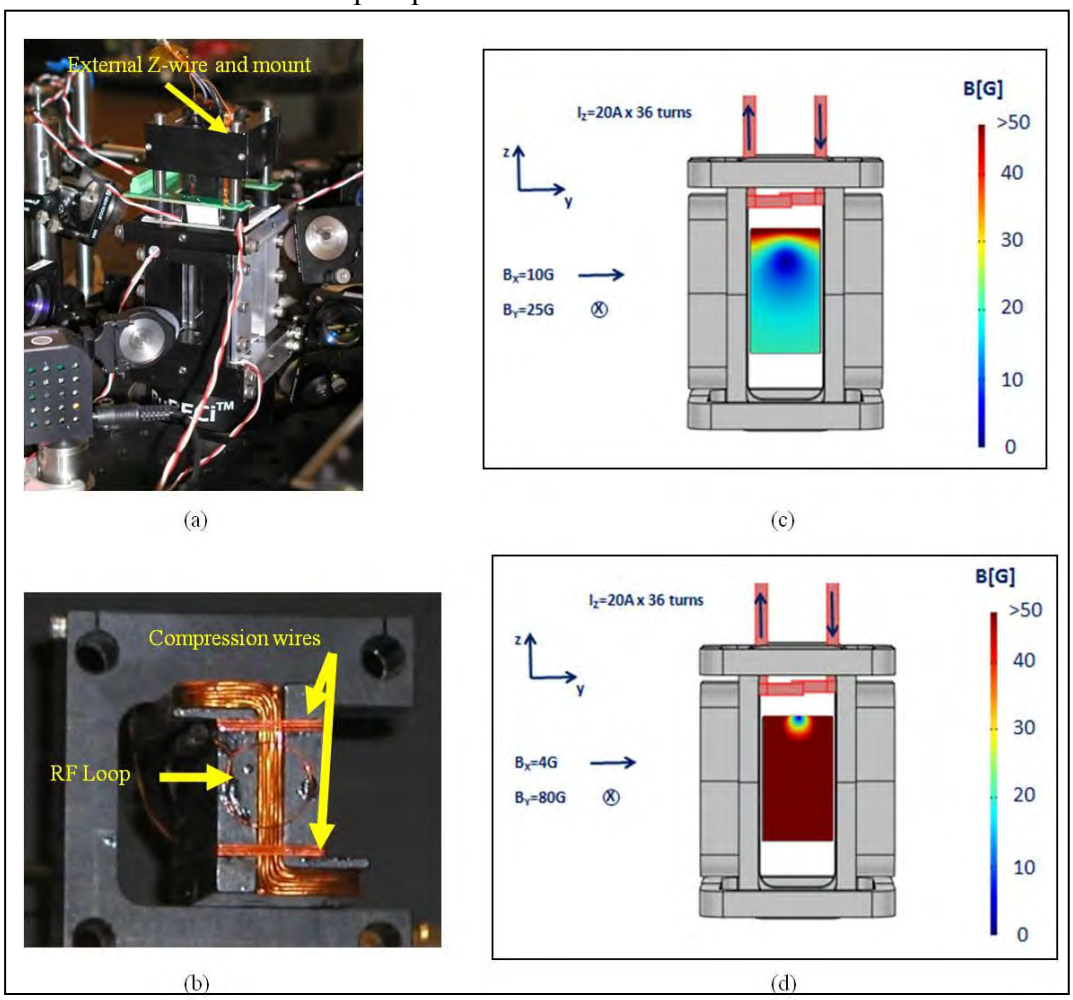

Figure 12. (a) Overall view of the external z-wire configuration. (b) Close up view of the portion of the wire that faces the top of the atom chip. Also shown is the wire loop that is used for RF forced evaporation as discussed in Section 3.4 below. Finite element model of the magnetic field generated along the center of the upper cell (c) just after transfer from CMOT and (d) just before transfer to atom chip trap.

Transfer of atoms the purely magnetic external z-wire trap begins by ramping the 3-D MOT field from ~10 G/cm to 30 G/cm and simultaneously increasing the cooling laser detuning from –2Γ to –5Γ, where Γ = 2π 6 MHz is the natural line-width. This stage is known as the compressed MOT or CMOT and lasts ~30 ms. The CMOT stage results in an order of magnitude increase in the cloud density. A bias field along the z-axis is then ramped up in order to move the cloud to its final position for capture in the external z-wire trap. Before transfer the 3-D MOT fields are turned off and the cooling laser further detuned to –10 Γ for a period of 3–10 ms of polarization gradient cooling which reduces the cloud temperature to ~40 μK. The cooling light is left on for

~100 μs after the repump light is turned off to pump atoms into the |F=1, mf=-1> magnetically trappable state. Figure 13 is an absorption image of the atom cloud just after compression and optical molasses stages. From the CMOT stage on we use absorption imaging exclusively for characterizing the number and temperature of atoms in the cloud and for imaging the interference fringes. In absorption imaging a weak (2–10 μW), circularly polarized, resonant laser beam is passed through the atom cloud and into the imaging camera for a short (~30–150 μs) time. Three images are actually taken for the absorption image, one image with atoms and probe beam light (atoms image), one image of the probe beam only (probe image), and one image without probe beam or atoms (background). The optical density of the cloud is then given by,

$$O.D. = Ln\left[\frac{atoms\ image - background}{probe\ image - background}\right] \tag{7}$$

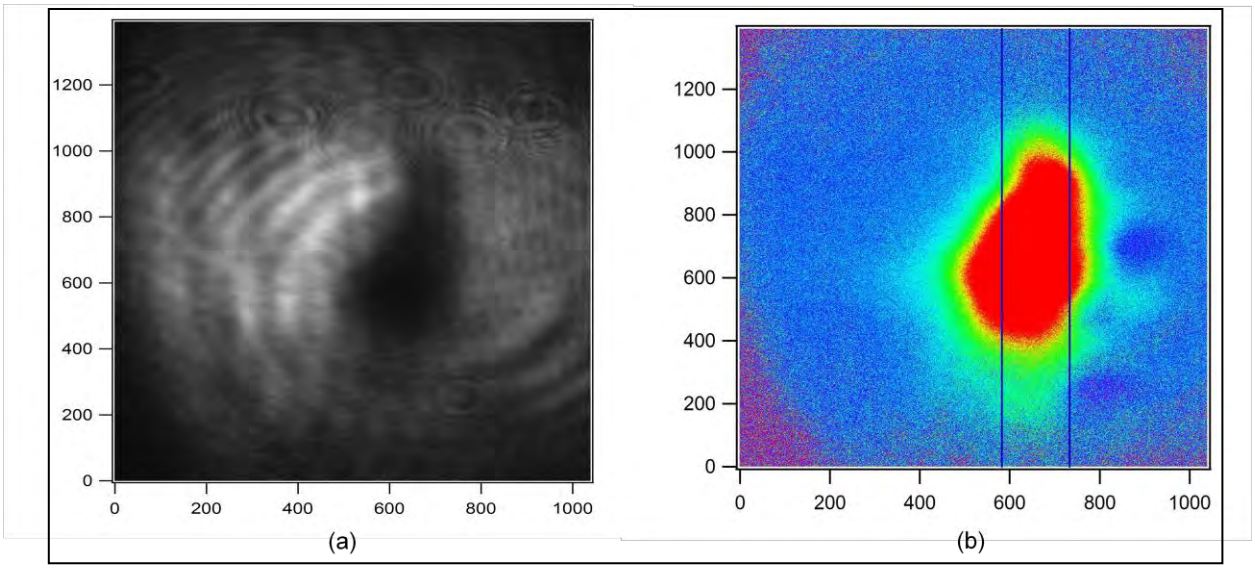

Figure 13. (a) Raw absorption image and (b) optical density calculated from equation (7).

The number of atoms in the cloud is then related to the optical density of the cloud by,

$$N_{atoms}^{absorption} = \frac{\pi\, w_y w_z O.D.}{\sigma} \tag{8}$$

where $w_{y,z}$ are the Gaussian widths of the cloud in the plane of the image and σ is the ^{87}Rb D_2 line absorption cross-section for circularly polarized light (~3×10^{-9} cm^2). Finally, the current in the external z-wire is ramped up to ~20 A and x and y bias fields are added complete the transfer of the atoms to the purely magnetic external z-wire trap. Figure 14 shows an absorption image (a) and density profile (b) for ~10^6 atoms in the external z-wire trap.

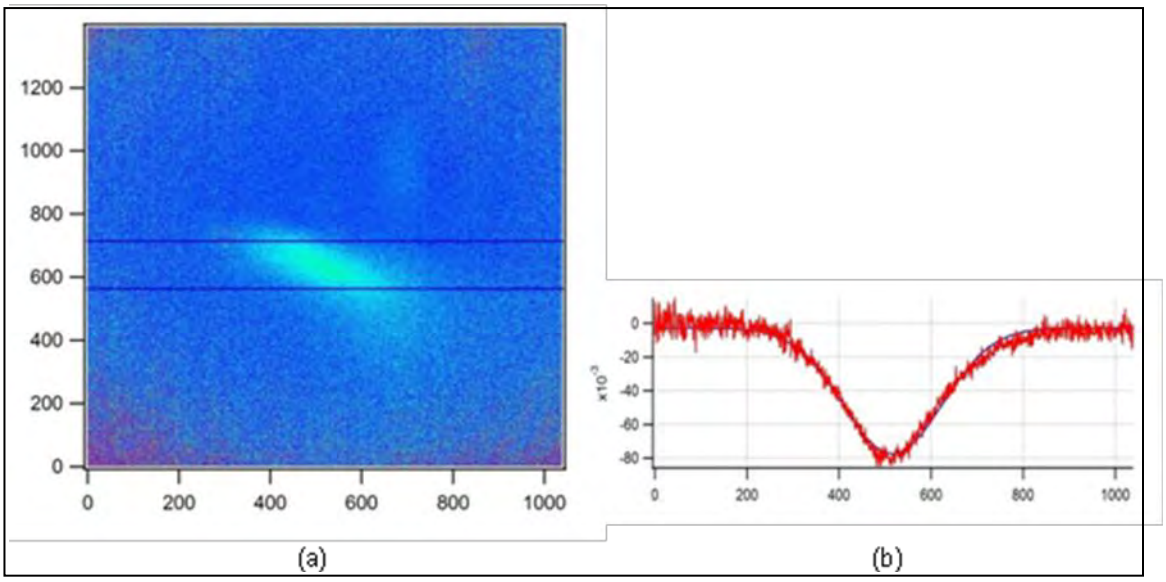

Figure 14. Absorption image (a) and density profile (b) for ~10^6 atoms in the external z-wire trap.

3.4 Atom Chip Trap and Waveguide

The 26mm x 26mm atom chip currently used in our system is formed by depositing 100 µm-wide, 10 µm-thick copper conductors onto a 450 µm-thick silicon substrate. A wire segment in a Z configuration, shown in red on the chip wire layout in figure 15 (a) is used with external bias fields to create the waveguide potential. This trap has a large trap frequency in the radial direction, typically ~2 kHz, but a much lower frequency along the axis of the waveguide, typically ~10 Hz. During the evaporative cooling sequence discussed below higher trap frequencies are obtained with a dimple trap that is formed by passing current through a cross wire, shown in purple. As seen in figure 15 (b) the atom chip is anodically bonded to the quartz cell and serves as a vacuum seal. Current is provided to the wires by hermetically sealed UHV through-chip vias. Once atoms are successfully transferred from the external z-wire trap to the chip waveguide, current in the cross-wire, in purple in figure 15 (a) is ramped up to create a much tighter dimple trap. Both magnetic field and current simulations of the waveguide and dimple trap are shown in figure 16. Once in this dimple trap, the atoms are further cooled by radio frequency forced evaporation (*4*). The atoms can then be released by lowering the trap frequency in one dimension and experiments in atom optics can then be performed.

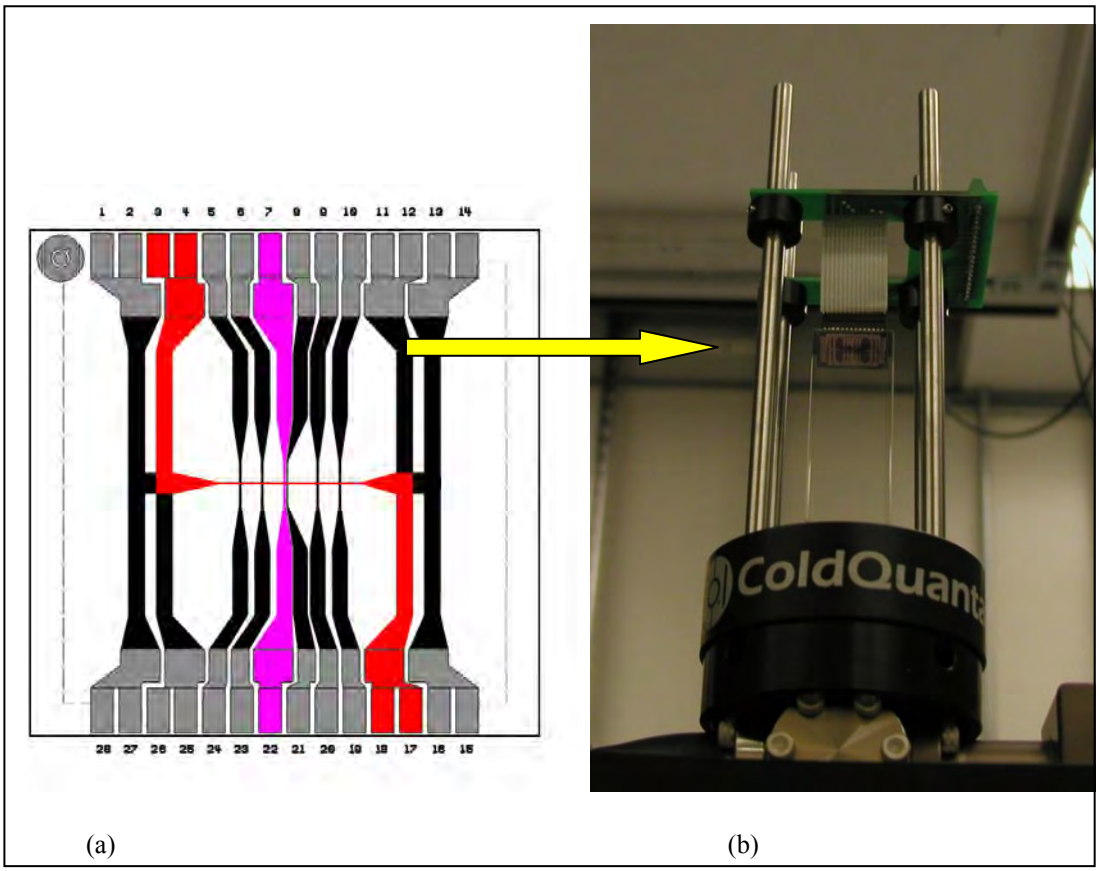

Figure 15. (a) A wire segment in a Z configuration, shown in red is combined with external bias fields to create an Ioffe-Pritchard trap. Higher trap frequencies used during evaporative cooling are obtained with a dimple trap that is formed by passing current through a cross wire, shown in purple. (b) View of the upper vacuum cell with the various coil mounts removed. The atom chip is anodically bonded to the quartz and serves as a vacuum seal.

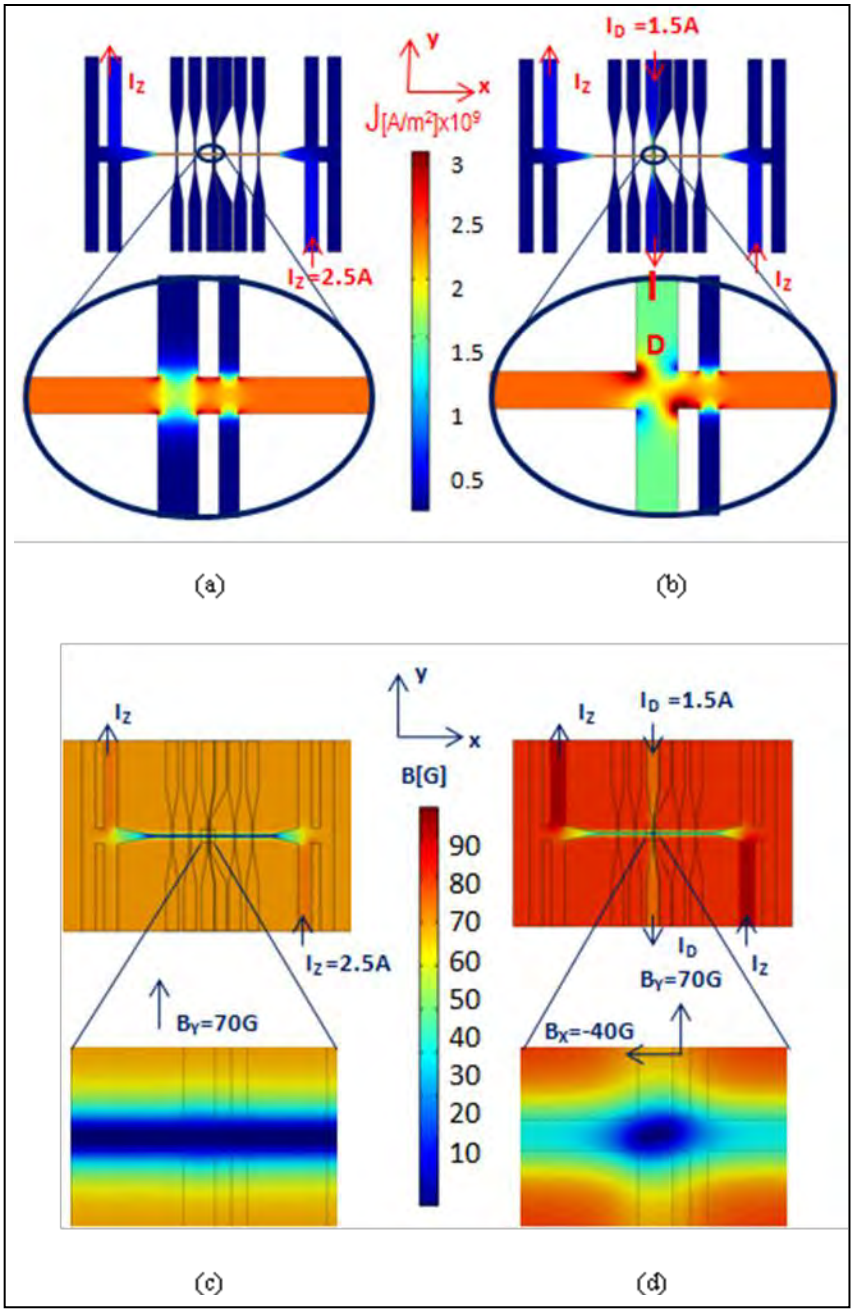

Figure 16. Finite element model of the current distribution (a, b) and resulting magnetic field (c, d) in the chip wave-guide and dimple trap.

4. Conclusions

In this report we have described our experimental apparatus in detail and discussed the current progress towards interferometric measurements with clouds of ultra-cold atoms on a chip. The successful use of atom chip based interferometers as inertial sensors has been hindered by the

ability to split the atom beam into coherent parts and have an effective means of reading out the phase information. The overall focus of our research program is to overcome these technical challenges and implement atom chip interferometers using clouds of BEC atoms. Presently we are optimizing the transfer to the atom chip trap as well as our resolution for absorption imaging of clouds of ultracold atoms. Initial experiments with the atom chip waveguide and related numerical modeling will be the focus of future reports.

5. References

1. Born, M. *Atomic Physics* 5th Ed. Blackie and Son Limited, London, 1951.
2. Anderson, M. H.; Ensher, J. R.; Matthews, M. R.; Wieman, C. E.; Cornell, E. A. *Science* **269**, *5221*, 1995.
3. Metchalf, H. J.; van der Straten, P. *Laser Cooling and Trapping* Springer, Berlin, 1999.
4. Ketterle, W.; Van Druten, N. J. Advances In Atomic, Molecular, and Optical Physics. **1996**, *37*, 181.
5. Gustavson, T. L.; Bouyer, P.; Kasevich, M. A. *Phys. Rev. Lett.* **1997**, *78*, 2046.
6. Gustavson, T. L.; Landragin, A.; Kasevich, M. A. *Class. Quantum Grav.* **2000**, *17*, 2385.
7. Fortágh, J.; Zimmermann, C. *Rev. Mod. Phys.* **2007**, *79*, 235.
8. Adapted from http://www.coldquanta.com/products.htm
9. Hänsch, T. W.; Schawlow, A. L. *Optics Communications* **1975**, *13*, 68.
10. Images from California Institute of Technology lab manual, available at http://www. its,.caltech.edu/~ph76a/.
11. Dieckmann, K.; Spreeuw, R.J.C.; Weidem¨uller, M.; Walraven, J.T.M. *Physical Review A* **1998**, *58*, 3891.
12. Steck, Daniel A. Rubidium 87 D Line Data," available online at http://steck.us/alkalidata (revision 2.1.4, 23 December 2010).

NO. OF COPIES	ORGANIZATION
1 PDF	DEFENSE TECH INFO CTR ATTN DTIC OCA 8725 JOHN J KINGMAN RD STE 0944 FT BELVOIR VA 22060-6218
1	DARPA ATTN J ABO-SHAEER 3701 N FAIRFAX DR ARLINGTON VA 22203-1714
1 CD 1 HC	US ARMY RSRCH OFC ATTN P BAKER (1 CD, 1 HD) PO BOX 12211 RESEARCH TRIANGLE PARK NC 27709-2211
1 CD 4 HCS	DEPT OF THE ARMY WEAPONS SCIENCES DIRECTORATE ATTN AMSRD AMS WS H EVERITT ATTN AMSRD AMS WS K MYNENI ATTN AMSRD AMS WS P REYNOLDS (1 CD, 1 HC) ATTN AMSRD AMS WS T BAHDER REDSTONE ARSENAL AL 35898-5000
38	US ARMY RSRCH LAB ATTN IMNE ALC HRR MAIL & RECORDS MGMT ATTN RDRL CIO LL TECHL LIB ATTN RDRL CIO MT TECHL PUB ATTN RDRL SEE O P LEE ATTN RDRL SEE O P PELLEGRINO ATTN RDRL SEE O W M GOLDING (30 HCS) ATTN RDRL SER E F CROWNE ATTN RDRL SES E H BRANDT ATTN RDRL SES P A EDELSTEIN ADELPHI MD 20783-1197